

Lagrangian intermittency and vertical confinement in stably stratified turbulence

Arun Kumar Varanasi^{1, a)}

International Centre for Theoretical Sciences, Tata Institute of Fundamental Research, Bengaluru 560089, India

(Dated:)

We investigate the Lagrangian properties of homogeneous, stratified turbulence at different Brunt-Väisälä frequencies. We show increasing vertical confinement of trajectories with increasing stratification strength highlighting the predominantly horizontal dynamics of these flows. We characterize the intermittent properties of the fluid motion by computing the probability distributions of the horizontal and vertical Lagrangian velocity increments and Lagrangian horizontal velocity structure functions, and find that horizontal velocity differences display intermittency at higher orders. Our results provide an understanding of the Lagrangian dynamics in stratified turbulence, and highlight the importance of buoyancy forces in shaping the Lagrangian statistics in these flows.

Keywords: Stratified turbulence, Lagrangian intermittency, Geophysical flows

An understanding of the small-scale physics of the ocean and atmosphere is closely tied to our understanding of mixing and transport processes in these planetary systems^{1,2}. These issues typically reduce to important questions on the dynamics of *suspended particles* in such flows. For example, the core of a cloud can be modeled reasonably as *just a* (dilute) suspension of ice crystals and water droplets. A drastic but useful simplification is to approximate the carrier flow using theoretically tractable simple models. Examples of such flows include shear, simple vortical, laminar, and smooth but chaotic flows. However both oceanic and atmospheric flows are notoriously turbulent. By construction simpler model flows share the same *smoothness* of turbulence at the particle scale. What they lack however is a key feature of turbulence namely intermittency^{3,4}. The intermittent nature of homogeneous and isotropic turbulence shows itself, for example, in the large tails of the distributions of spatial (Eulerian) and temporal (Lagrangian) velocity increments as well as velocity gradients. While a theory for intermittency starting with the incompressible Navier-Stokes equation remains elusive, the evidence that flows are intermittent have been documented in numerical simulations⁵⁻⁷, observations⁸ and experiments⁹. This deviation from Gaussian distributions has a striking manifestation in the strong deviation (from theoretical estimates) of the scaling exponents associated with the Eulerian and Lagrangian structure functions of velocity increments¹⁰. Given the complexity of turbulence, it is legitimate to ask whether *turbulence* matters when investigating the small-scale physics of mixing and transport. Recent studies suggest that the answer is yes. For example, the rate at which water droplets in a warm cloud coalesce and hence grow to sizes which precipitate is a direct outcome of the flow being turbulent and hence intermittent¹¹⁻¹⁴. These are important results and underline the fact that turbulence cannot be neglected to understand such phenomena in the atmospheric, oceanic and geophysical contexts. Furthermore, while fluid intermittency remains one of the outstanding questions of turbulence, it is only recently that

we have begun to fully appreciate its leading order contribution to problems which have a more direct bearing beyond the somewhat more conceptual challenges of mathematics or statistical physics.

Homogeneity, isotropy and constant density are of course (often justifiable at small scales) simplifications: Real atmospheric and oceanic flows are density stratified. While there have been several studies of stratified turbulence¹⁵⁻²¹, especially in the marine context with the allied, fundamental questions of carbon sequestration and marine snow, for example, the intermittent nature of homogeneous, stratified — and hence anisotropic — flows have received far less attention than what it perhaps deserves. As we discussed above, work on transport and mixing in homogeneous, isotropic and constant density incompressible turbulence shows that a proper understanding of phenomena such as collisions, coalescences, and gravitational settling of sediments — just as important in stratified turbulence — must factor in the intermittent nature of the carrier flow. Hence, in this paper we undertake the characterisation of the Lagrangian intermittency of stratified turbulence and leave the question of how it affects, for example, the concentration field of microorganisms and marine snow, for future work.

As is clear from the discussion above, for problems involving stratified media the flow needs to be modeled beyond the constant density Navier-Stokes equation²². Typically, density stratification is chosen to be linear but when such flows are driven (by an external force) to a turbulent state, fluctuations in the density field (ρ) naturally arise. Hence, by assuming a Cartesian coordinate system where the gravity $-g\hat{z}$ acts downward along the vertical \hat{z} axis, a density profile $\rho = \rho_0 - \gamma z + \rho_f$ mimics a stratified turbulent fluid; in the absence of turbulence, $\rho_f = 0$, leading to a stable stratification where the density decreases linearly with height, at a rate γ , along the vertical direction.

Momentum conservation ensures that the incompressible velocity field \mathbf{u} satisfies

$$\rho \left[\frac{\partial \mathbf{u}}{\partial t} + \mathbf{u} \cdot \nabla \mathbf{u} \right] = -\nabla p_0 + \mu \nabla^2 \mathbf{u} - \rho g \hat{z} + \mathbf{F} \quad (1)$$

^{a)}Electronic mail: arun.target@gmail.com

where p_0 is the pressure field, μ is the bulk viscosity and \mathbf{F} is an external drive. In the ideal, inviscid $\mu = 0$, unforced $\mathbf{F} = 0$ limit, any displacement of a parcel of fluid will lead to its oscillations with a natural, Brunt-Väisälä frequency $N = \sqrt{\frac{g\gamma}{\rho_0}}$. Further, by taking the Boussinesq approximation of replacing ρ with ρ_0 in the right hand side of Eq. (1), and setting $p = p_0 + \rho_0 g z - \frac{\gamma g z^2}{2}$, we obtain (with the forcing term \mathbf{f} normalised by the density)

$$\frac{\partial \mathbf{u}}{\partial t} + \mathbf{u} \cdot \nabla \mathbf{u} = -\frac{\nabla p}{\rho_0} + \nu \nabla^2 \mathbf{u} - \frac{N^2 \rho_f}{\gamma} \hat{\mathbf{z}} + \mathbf{f} \quad (2)$$

In a non-quietescent flow, the density field ρ follows an advection-diffusion equation with a diffusion constant κ . However, it is useful to work, instead of the density field, with its surrogate, the buoyancy field $b = \frac{\rho_f N}{\gamma}$. This buoyancy field has the added advantage of being dimensionally the same as the velocity field. By rewriting the advection-diffusion equation of ρ in terms of b and rewriting the buoyancy term in Eq. (2) in terms of b , we arrive at the final set of coupled, equations which describe a (turbulent) stratified flow

$$\frac{\partial \mathbf{u}}{\partial t} + \mathbf{u} \cdot \nabla \mathbf{u} = -\nabla p + \nu \nabla^2 \mathbf{u} - N b \hat{\mathbf{z}} + \mathbf{f}; \quad (3)$$

$$\frac{\partial b}{\partial t} + \mathbf{u} \cdot \nabla b = \kappa \nabla^2 b + N \mathbf{u} \cdot \hat{\mathbf{z}}; \quad (4)$$

along with the incompressibility constraint

$$\nabla \cdot \mathbf{u} = 0; \quad (5)$$

The external force \mathbf{f} drives the system to a statistical steady, homogeneous but anisotropic turbulent state for a suitable choice of parameters. As discussed earlier, the anisotropy along the vertical direction $\hat{\mathbf{z}}$ leads to distinct statistical behavior when measured in planes along the Z -axis to those measured on the XY plane perpendicular to $\hat{\mathbf{z}}$. To differentiate between these two directions, it is convenient to express quantities using the superscripts \perp for components measured along the vertical direction and \parallel for the component measured in the planes perpendicular to the $\hat{\mathbf{z}}$. For instance, the velocity field \mathbf{u} can be decomposed in to components \mathbf{u}^\perp and \mathbf{u}^\parallel .

The sensitivity of the flow to stratification is determined by the competition between the buoyancy and inertial forces in Eq. (3). Thence, the degree of stratification is characterised by the non-dimensional Froude number $Fr = \frac{u_{\text{rms}}}{L_{\text{int}} N}$ obtained from a simple ratio of inertial-to-buoyancy forces; here u_{rms} is the root-mean-square velocity, and L_{int} is the integral (large) length scale of the flow. The integral length scale is most conveniently expressed in terms of the energy spectrum $E(k)$ of turbulence through $L_{\text{int}} = \frac{\int_0^\infty k^{-1} E(k) dk}{\int_0^\infty E(k) dk}$.

Just at the Froude number gives us a measure of the strength of stratification, the degree of turbulence is determined by the non-dimensional Reynolds number which is a measure of the ratio of the inertial to dissipative forces in Eq. (3). Typically, this measure is the Taylor-scale-based Reynolds number $Re_\lambda = u_{\text{rms}}^2 \sqrt{15} / \epsilon_k \nu$ where ϵ_k is the mean kinetic energy dissipation rate of the flow. Finally, the contrast between

the fluid viscosity and density diffusivity is set by the Prandtl number $Pr = \nu / \kappa$. Strongly stratified turbulence implies that the buoyancy Reynolds number $Re_b \sim (Re_\lambda Fr)^2 > 1$ and $Fr \ll 1$ along with $Re_\lambda \gg 1$.

Finally, the Brunt-Väisälä frequency $N = \sqrt{\frac{g\gamma}{\rho_0}}$ has dimensions of inverse time. In order to make comparisons between our simulations and observations meaningful, we define a non-dimensional form of this frequency $\tilde{N} \equiv \tau_\eta N$, where $\tau_\eta \equiv \sqrt{\frac{\nu}{\epsilon}}$ is the characteristic short (Kolmogorov) time-scale of the underlying flow.

To have a sense of these numbers in what follows, it is useful to have an estimate of the key parameters defining strongly stratified turbulence in, for example, an ocean. Indeed, it is well known that there exists huge variations in the typical velocity, stratification and dissipation rates across the ocean and at different depths. Nevertheless, in a typical ocean, it is known that the $\mathcal{O}(10^{-3} \text{sec}) \lesssim N \lesssim \mathcal{O}(10^{-1} \text{sec})$. Given that $\tau_\eta \sim 1 \text{sec}$ (since for sea water $\nu = 10^{-6} \text{m}^2/\text{sec}$ and $\epsilon_k \approx 10^{-6} \text{m}^2/\text{sec}^3$), the normalised frequency also varies as $\mathcal{O}(10^{-3}) \lesssim \tilde{N} \lesssim \mathcal{O}(10^{-1})$. Observations suggest that $0.1 \text{m/sec} \lesssim u_{\text{rms}} \lesssim 2.0 \text{m/sec}$ and $\mathcal{O}(10^4) \text{m} \lesssim L_{\text{int}} \lesssim \mathcal{O}(10^5) \text{m}$; hence the Froude numbers range as $\mathcal{O}(10^{-4}) \lesssim Fr \lesssim \mathcal{O}(10^{-2})$ and $Re_\lambda \sim \mathcal{O}(10^3)$. Finally, the Prandtl number can vary from $Pr \sim 7$ (thermal stratification) to as high as 700 (salt stratification). In the fully developed turbulent regime, it is reasonable to assume $Pr \sim 1$.

The equations governing stratified turbulence are solved by using direct numerical simulations (DNSs) of Eqs. (3)-(5). The simulations are performed using a pseudo-spectral method, on a triply periodic cube of side length 2π , which is discretized into 512^3 collocation points. We use a second-order Runge-Kutta method for time-marching. The flow is driven to a non-equilibrium, statistically stationary through a constant energy injection force \mathbf{f} limited to the first two wavenumber shells ($k \leq 2$), and applied only to the horizontal scales. A constant kinematic viscosity of $\nu = 5 \times 10^{-3}$ and the constant energy injection $\epsilon = 0.9$ ensures, in the steady state, the flow achieves a Taylor-scale Reynolds number $Re_\lambda \approx 140$. We conduct simulations for different normalized Brunt-Väisälä frequencies, $\tilde{N} = 0.28, 0.35, 0.42, 0.49$ and 0.56 . These correspond to Froude numbers are $Fr = 0.238, 0.182, 0.158, 0.143$ and 0.126 . The Prandtl number is set to unity across all simulations.

It is important to emphasize that the Froude numbers and (normalised) Brunt-Väisälä frequencies in our simulations falls well within the range observed in oceanic environments. Nevertheless, the range of values is constrained by the computational resources currently available to us. It is easy to check, however, that all our simulations are within the strongly stratified regime with $Re_b \gg 1$, $Fr \ll 1$ and $Re_\lambda \gg 1$.

The density stratification and hence the emergent buoyancy force lead to a vertical confinement of fluid elements. The restraint on the motion of vertical mixing of fluid elements are accentuated with increasing Brunt-Väisälä frequencies. This confinement is most easily seen when tracking fluid elements through Lagrangian tracers seeded in the flow, once a statistically steady, non-equilibrium state is reached. Such

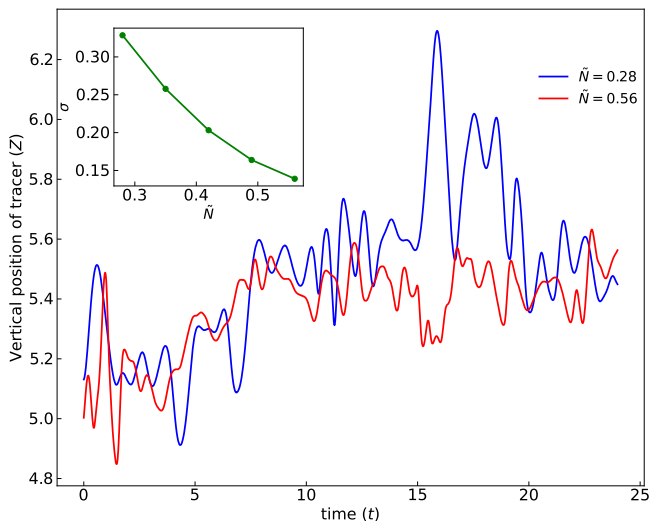


FIG. 1: Time evolution of vertical position ($Z(t)$) for a tracer at extreme normalized Brunt-Väisälä frequencies $\tilde{N} = 0.28$ and $\tilde{N} = 0.56$. Increasing \tilde{N} suppresses the fluctuations and tend to confine the tracers vertically. The inset quantifies this effect, showing the standard deviations of the vertical fluctuations decreasing with \tilde{N}

a point-like, massless tracer particle, characterised by its instantaneous position \mathbf{x} and velocity \mathbf{v} vectors, follows the Lagrangian dynamics

$$\frac{d\mathbf{x}}{dt} = \mathbf{v}; \quad \mathbf{v} = \mathbf{u}(\mathbf{x}, t). \quad (6)$$

In our simulations, to obtain reliable statistics, we seed 10^5 Lagrangian particles and numerically solve for the trajectories defined above by using a second-order Runge-Kutta scheme. The fluid velocity $\mathbf{u}(\mathbf{x}, t)$, at the typically off-grid Lagrangian position \mathbf{x} is obtained through a trilinear interpolation from the regular, periodic Cartesian grid on which the Euler velocity (and density) field equations are solved.

In Fig. 1, we show representative plots of the vertical position Z of a randomly selected tracer trajectory from simulations with the smallest $\tilde{N} = 0.28$ and largest $\tilde{N} = 0.56$ (normalized) Brunt-Väisälä frequencies. The visual evidence of stronger confinement and subdued fluctuations with increasing \tilde{N} is of course suggestive but hardly conclusive. To see if this is indeed the case, we calculate, for a given \tilde{N} and particle, the mean vertical position \bar{z} and hence a measure of the fluctuations through the standard deviation $\sigma = \langle [z - \bar{z}]^2 \rangle$, where the angular brackets $\langle \cdot \cdot \rangle$ denotes an average over all 10^5 trajectories.

In the upper inset of Fig. 1, we plot σ vs \tilde{N} and, as anticipated, we find increasing confinement as the flow becomes more stratified with increasing \tilde{N} . Using this, we compute the probability density functions of the normalised vertical displacements $\tilde{z} \equiv \frac{z - \bar{z}}{\sigma}$ and are shown in Fig. 2. The PDFs exhibit distinct non-Gaussian features and collapse onto a common curve. For comparison, we also plot a Gaussian distribution, highlighting the deviations from Gaussianity, partic-

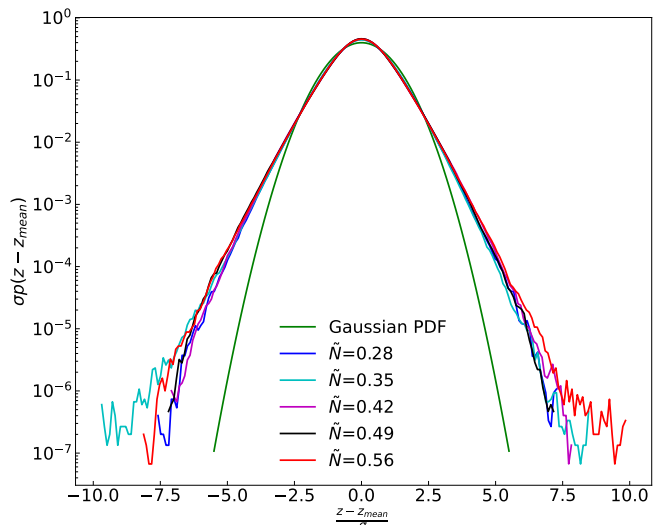


FIG. 2: Probability distribution functions (PDFs) of normalized vertical displacements ($\frac{z - z_{\text{mean}}}{\sigma}$) for different stratification strengths \tilde{N} . The data collapse onto a universal curve, highlighting the scale-independence in strongly stratified turbulence. Deviations from the Gaussian distribution (green curve) reveal non-Gaussian tails, suggesting intermittent vertical mixing.

ularly in the tails of computed PDFs. The collapse for different \tilde{N} also highlights the underlying statistical structure of the vertical confinement in the strongly stratified turbulence regime.

How does this effect of vertical confinement show up in the (vertical) mean square displacement (MSD) of trajectories? We define the $\Delta z^2 = \langle \|z(t) - z(0)\|^2 \rangle$, where the angular brackets $\langle \cdot \rangle$ denote an ensemble averaging over all trajectories and $\|\cdot\|$ the Eulerian norm. We expect Δz^2 to show a ballistic scaling τ^2 (where we use non-dimensional time $\tau = t/\tau_\eta$) for short times and up to separations $\Delta z^2 \sim z_*^2$. This ballistic regime is clearly seen in Fig. 3 which terminates at a Brunt-Väisälä frequency dependent length scale z_* . From physical grounds it is reasonable to assume that this ballistic regime persists up to length scales z_* which are comparable to the intrinsic buoyancy scale ℓ_B of the flow. The buoyancy length scale is estimated, dimensionally, from the root-mean-square vertical fluid velocity u_z^{rms} via $\ell_B \sim \frac{u_z^{\text{rms}}}{N}$. In order to test this hypothesis, we show a plot of z_* , estimated from plots of Δz^2 , vs ℓ_B in the upper inset of Fig. 3. The reasonable compelling linear relation between the two confirms our conjecture $z_* \approx \ell_B$. Beyond z_* , and at longer times, the MSD shows distinct sub-diffusive behaviour as is easily seen when compared to the $\Delta z^2 \sim t$ line drawn in Fig. 3 as a guide to the eye.

Is it reasonable to conjecture that the transition from the ballistic to the sub-diffusive regime is set by the timescale $\tau_b = 2\pi/N$ associated with the typical time period of the oscillatory fluid elements in the vertical direction. This would suggest that the MSD plots shown in the main panel of Fig. 3 ought to collapse on rescaling time with τ_b (and Δz^2 by ℓ_B^2).

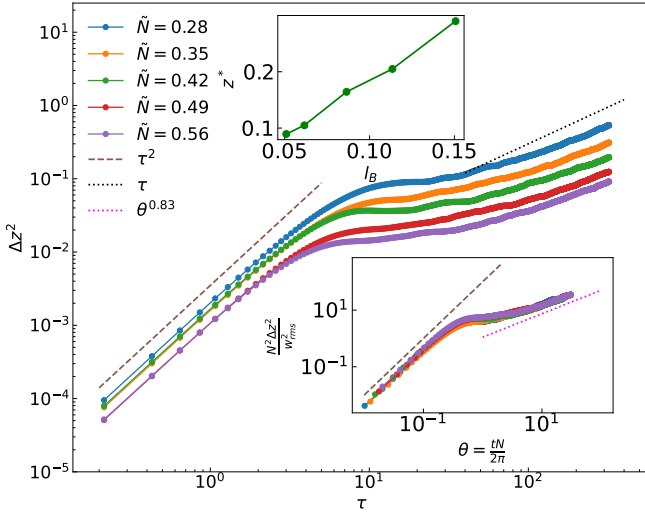


FIG. 3: Vertical mean square displacement (MSD) of tracer particles as a function of the rescaled time ($\tau = \frac{t}{\tau_\eta}$). The main panel shows the ballistic regime ($\Delta z^2 \sim \tau^2$) at short times, transitioning to a sub-diffusive regime at longer times. The upper inset presents the estimated transition length scale (z^*) against the buoyancy scale (l_B). The upper inset displays the MSD curves rescaled by τ_B and l_B^2 , revealing a universal sub-diffusive scaling regime, θ^ξ with $\xi = 0.83$.

In the lower inset of Fig. 3 we show plots of the MSD (as in the main panel) but on such rescaling. Furthermore, such rescaled plot suggest a clear sub-diffusive regime $\Delta z^2 \sim \theta^\xi$, with $\xi \approx 0.83$ for all Brunt-Väisälä frequencies. Here, we have denoted the rescaled time as $\theta = \frac{tN}{2\pi}$. (Our calculations for the MSD on the horizontal planes are in agreement to those reported earlier by van Aatrijk, Clercx, and Winters²³.)

We now turn our attention to the Lagrangian velocity statistics to uncover how intermittent such flows are and their dependence on the Brunt-Väisälä frequency. We begin by examining the Lagrangian velocity increments separately for the vertical and horizontal components of the velocity field. These increments are defined, respectively, as $\Delta v^\perp \equiv v_z(t + \Delta t) - v_z(t)$ and $\Delta v^\parallel \equiv (v_x(t + \Delta t) - v_x(t)) + (v_y(t + \Delta t) - v_y(t))$. In the insets of Fig 4 we show the corresponding probability density functions (a) \mathcal{P}^\perp and (b) \mathcal{P}^\parallel for three different (normalised) time increments $\Delta\tau = \frac{\Delta t}{\tau_\eta}$. While for large $\Delta\tau$ we expect the distributions to approach a Gaussian, the nature of these distributions for small $\Delta\tau$ holds the key to the nature of Lagrangian intermittency in strongly stratified turbulence. The insets of Figures 4(a) and (b) show clear non Gaussian, and ever widening tails of the distributions as $\Delta\tau \rightarrow 0$. Such non Gaussian tails are typically signatures of Lagrangian intermittency which are quantified through a measure of the kurtosis for both the vertical $\kappa^\perp = \frac{\langle (\Delta v^\perp)^4 \rangle}{\langle (\Delta v^\perp)^2 \rangle^2}$ and in-plane $\kappa^\parallel = \frac{\langle (\Delta v^\parallel)^4 \rangle}{\langle (\Delta v^\parallel)^2 \rangle^2}$ components. In the main panels of

Fig. 4 we show plots of (a) κ^\perp and (b) κ^\parallel vs the normalised time increment $\Delta\tau$. Clearly as $\Delta\tau \rightarrow 0$, and taking the value

of kurtosis as a surrogate for the degree of intermittency, the in-plane Lagrangian motion appears to be more intermittent than its vertical component as a possible consequence of the confinement discussed before with κ^\perp and κ^\parallel increasing with \tilde{N} as $\Delta\tau \rightarrow 0$.

Finally, we make use of the measurements reported in Fig. 4 to calculate the p -order, Lagrangian structure functions $S_p^\parallel \equiv \langle (\Delta v^\parallel)^p \rangle$ and $S_p^\perp \equiv \langle (\Delta v^\perp)^p \rangle$. The quenched motion in the vertical direction suggests that the horizontal dynamics dominate the flow leading to a power law scaling of the form $S_p^\parallel \sim \Delta\tau^{\zeta_p^\parallel}$. This scaling holds for $1 \lesssim \Delta\tau \lesssim 40$ corresponding to the inertial range of the horizontal dynamics. For smaller $\Delta\tau$, the structure functions are expected to follow a simple scaling derived from the Taylor expansion. For $\Delta\tau$ beyond the inertial range, the structure functions ought to saturate.

From the dimensional analysis, we expect that horizontal structure functions should scale as $S_p^\parallel \sim (\epsilon\Delta\tau)^{p/2}$ in the inertial range in the absence of intermittency, which correspond to scaling exponents $\zeta_p^\parallel = p/2$. To test this scaling behavior, we plot the sixth order structure function S_6^\parallel against $\Delta\tau$ in Fig. 5. This figure also include two reference plots: the expected scaling in the limit of $\Delta\tau \rightarrow 0$ ($\zeta_6^\parallel = 6$), and the inertial range scaling ($\zeta_6^\parallel = 3$) in the absence of intermittency. While the small- $\Delta\tau$ data agree well with the $\zeta_6^\parallel = 6$ scaling, significant deviations from $\zeta_6^\parallel = 3$ emerge in the inertial range, demonstrating strong intermittency at this order. Similar behavior occurs for lower orders (not shown here), with decreasing intermittency effects as the order (p) reduces.

To further characterize the intermittency of the predominantly horizontal motion, we analyze the scaling exponent ratios $\zeta_p^\parallel/\zeta_2^\parallel$ using the extended self similarity (ESS)^{24,25} combined with local slope analysis. The local slopes are defined as: $\frac{\zeta_p^\parallel}{\zeta_2^\parallel}(\Delta\tau) = \frac{d \log(S_p^\parallel(\Delta\tau))}{d \log(S_2^\parallel(\Delta\tau))}$. Examining these slopes across varying time separations ($\Delta\tau$) provides insight into the accuracy and the scaling behavior of the exponents.

Fig. 6 shows the local slopes for the largest \tilde{N} ($= 0.56$) in our simulations. As time separations $\Delta\tau \rightarrow 0$, the local slopes approach $p/2$ consistent with Taylor-series expansion of the structure functions. As $\Delta\tau$ increases, the local slopes for $p > 2$ initially decrease – reflecting the influence of the vortical structures trapping the tracers²⁶ – before rising again due to inertial effects, a behavior also observed in homogeneous isotropic turbulence. A clear scaling range (highlighted in gray in Fig. 6) emerges at larger $\Delta\tau$, indicating power law scaling (with intermittency) in the exponent ratios. From this range, we extract $\zeta_p^\parallel/\zeta_2^\parallel$ and plot it against the order p in Fig. 7. The theoretical non-intermittent scaling (black line) is significantly deviated at higher orders, confirming intermittency in the horizontal Lagrangian velocity structure functions. These results suggest a multifractal nature of the predominantly horizontal flow, motivating future work on detailed multifractal analysis in stratified turbulence.

In addition to the horizontal Lagrangian velocity structure functions, we also examine their vertical velocity struc-

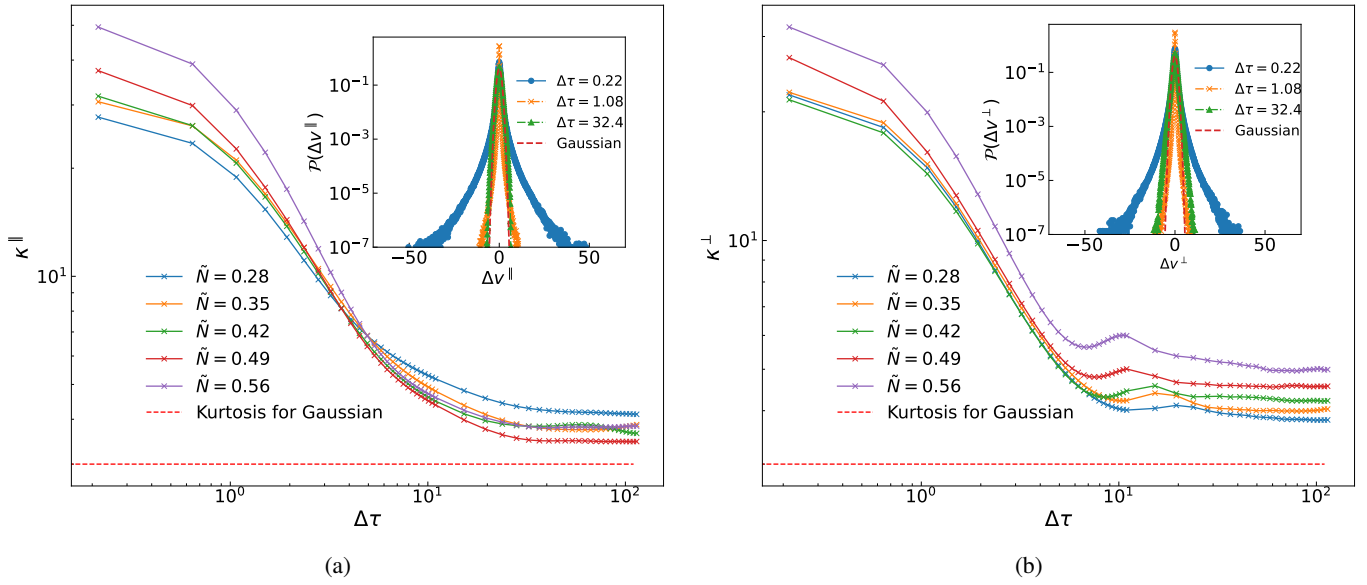


FIG. 4: Velocity increment statistics revealing intermittency in stratified turbulence. (a) Kurtosis κ^{\parallel} of horizontal velocity increments (Δv^{\parallel}) and (b) κ^{\perp} of vertical increments (Δv^{\perp}) versus normalized time increments ($\Delta\tau$); In the inset of each main panel, the corresponding PDFs (\mathcal{P}^{\parallel} and \mathcal{P}^{\perp}) at three $\Delta\tau$ values are shown for largest \tilde{N} ($= 0.56$). Widening non-Gaussian tails (insets) and elevated Kurtosis values at small $\Delta\tau$ demonstrate strong intermittency.

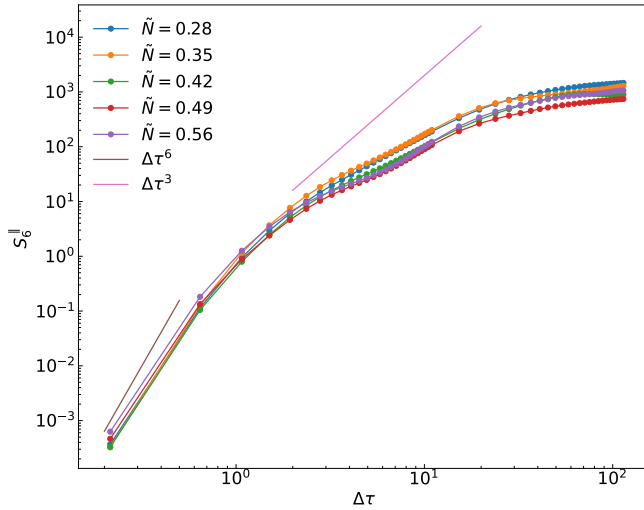


FIG. 5: Scaling behavior of the sixth order horizontal Lagrangian velocity structure functions (S_6^{\parallel}). The figure also includes reference lines indicating the expected scaling in the limit of $\Delta\tau \rightarrow 0$ ($\zeta_6^{\parallel} = 6$) and the inertial range scaling in the absence of intermittency ($\zeta_p^{\parallel} = 3$). The scaling from simulations show large deviation due to intermittency.

ture functions S_p^{\perp} . Unlike the horizontal structure functions, which exhibit power law scaling in the inertial range, the vertical counterparts show a distinct dependence on \tilde{N} . In the main panel of Fig. 8, we show S_1^{\perp} plotted against $\Delta\tau$; this indeed suggests that the peaks in S_1^{\perp} depend on \tilde{N} with the peaks appearing at \tilde{N} dependent $\Delta\tau$. To quantify this depen-

dence, we plot the maximums of S_1^{\perp} against \tilde{N} in the upper inset of Fig. 8. This suggest $\tilde{N}^{-3/4}$ scaling for S_1^{\perp} in a range where buoyancy forces are important. In lower inset of Fig. 8, we show S_1^{\perp} (rescaled by $N^{-3/4}$) against the time increments rescaled by buoyancy time scale ($\Delta\theta$) which indeed suggests a collapse of all the curves especially for $\Delta\theta \gtrsim 1$. The peaks too appear approximately the same $\Delta\theta$. The behavior of remaining Lagrangian vertical structure functions (not shown) follows a similar trend, with the scaling now given by $S_p^{\perp} \propto \tilde{N}^{-3p/4}$ for the $\Delta\theta \gtrsim 1$. This indicates that the vertical motion, while constrained by buoyancy forces, still exhibits a systematic dependence on \tilde{N} .

To summarize, our findings demonstrate that increasing stratification strength enhances vertical confinement of tracers, leading to predominantly horizontal motion. This underscores the need for a detailed investigation of Lagrangian velocity increments in the horizontal direction. Our analysis reveals that intermittency in stratified turbulence exhibits distinct characteristics compared to homogeneous isotropic turbulence. Specifically, in the strongly stratified regime considered here, horizontal Lagrangian velocity increments display extended self-similarity, with pronounced intermittency at higher orders. While computationally demanding, extending this study to higher Reynolds numbers Re_{λ} and smaller Fr values would provide further insights into the nature of intermittency in strongly stratified turbulence.

The present results contribute to the broader understanding of intermittency in stratified turbulence and its implications for particle transport, including heavy, active, and neutrally buoyant particles. Further investigation into these effects would enhance our comprehension of mixing and transport processes in geophysical and environmental flows. Addition-

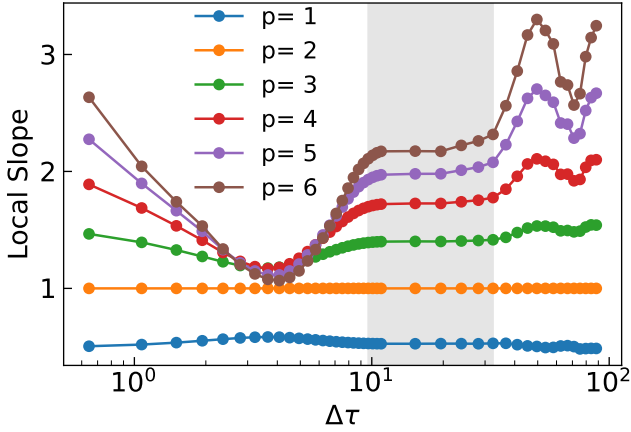


FIG. 6: Local slopes of ratios of the scaling exponents for horizontal velocity structure functions for $\tilde{N} = 0.56$. At small $\Delta\tau$, slopes approach $p/2$ (Taylor expansion limit). The emergence of a clear scaling range (in gray) at larger $\Delta\tau$ reveals power law behavior.

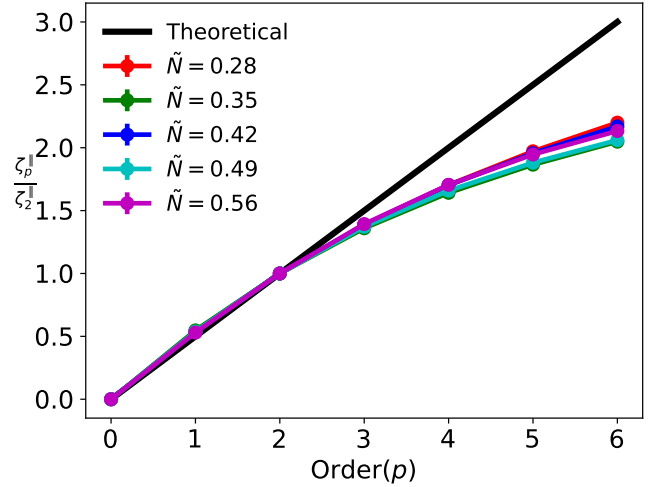


FIG. 7: Ratio of scaling exponents, $\frac{\zeta_p^{\parallel}}{\zeta_2^{\parallel}}$ versus order p for different \tilde{N} . Significant deviation from the theoretical non-intermittent scaling (black line) at higher orders confirms strong intermittency in horizontal Lagrangian velocities.

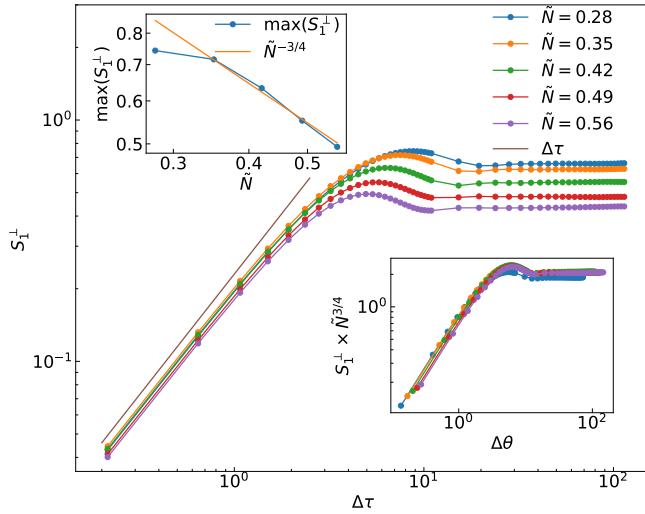


FIG. 8: Vertical Lagrangian velocity structure function S_1^{\perp} as a function of time increment $\Delta\tau$, showing \tilde{N} dependent peak values, while the lower inset demonstrates the collapse of rescaled S_1^{\perp} for $\Delta\theta \gtrsim 1$.

ally, a systematic study of Lagrangian tracer statistics, incorporating the effects of rotation and double diffusion, presents a promising avenue for future research. Complementary to this, examining intermittency in Eulerian statistics of horizontal velocity increments would establish a more comprehensive perspective on strongly stratified turbulence.

Building on these results, we will extend our work by analyzing the intermittency's role on the orientation statistics of spheroids in stratified turbulence motivated by recent

findings²⁷ on sedimenting spheroids in stratified fluids. Prior work on sedimenting spheroids in homogeneous isotropic turbulence has shown that the gravity induced inertial torque leads to non-gaussian orientation distributions localized about the broadside-on orientation²⁸. Stratification is expected to modify this behavior due to competing inertial and stratification torques that oppose each other in aligning spheroid axes²⁷. The underlying (stratified) turbulent torque can further modify this alignment. We will quantify these combined effects on the orientation statistics. In addition to the above, we will also investigate the elastic collisions between heavy (spherical) particles, which have been studied previously²⁹ in three dimensional random incompressible flow and we expect these collisions to become more prevalent in stratified turbulence.

ACKNOWLEDGMENTS

The author acknowledges Prof. Samridhhi Sankar Ray, ICTS-TIFR for his invaluable guidance, insightful discussions, and significant contributions to the development and writing of this manuscript. His feedback and criticism greatly improved the clarity of this work. The author also would like to thank Prof. Rama Govindarajan, ICTS-TIFR for many useful discussions. The simulations were performed on the ICTS clusters *Tetris* and *Contra*. This research was supported in part by the International Centre for Theoretical Sciences (ICTS) for participating in the programs — *Field Theory and Turbulence* (code:ICTS/ftt2023/12) and *Turbulence: Problems at the Interface of Mathematics and Physics* (code: ICTS/TPIMP2020/12). We acknowledge the support of the DAE, Govt. of India, under project no. 12-R&D-TFR-5.10-

1100 and project no. RTI4001.

- ¹S.A. Thorpe. *The Turbulent Ocean*. Cambridge University Press, 2005.
- ²Raffaele Ferrari and Carl Wunsch. Ocean circulation kinetic energy: Reservoirs, sources, and sinks. *Annual Review of Fluid Mechanics*, 41(1):253–282, 2009.
- ³U Frisch. *Turbulence: The Legacy of A. N. Kolmogorov*. Cambridge University Press, 1996.
- ⁴Uriel Frisch and Giorgio Parisi. Fully developed turbulence and intermittency. *New York Academy of Sciences, Annals*, 357:359–367, 1980.
- ⁵Eric D Siggia. Numerical study of small-scale intermittency in three-dimensional turbulence. *Journal of Fluid Mechanics*, 107:375–406, 1981.
- ⁶Samridhhi Sankar Ray. Non-intermittent turbulence: Lagrangian chaos and irreversibility. *Physical Review Fluids*, 3(7):072601, 2018.
- ⁷Rahul Pandit, Prasad Perlekar, and Samridhhi Sankar Ray. Statistical properties of turbulence: an overview. *Pramana*, 73:157–191, 2009.
- ⁸CW Van Atta and WY Chen. Structure functions of turbulence in the atmospheric boundary layer over the ocean. *Journal of Fluid Mechanics*, 44(1):145–159, 1970.
- ⁹George Keith Batchelor and Albert Alan Townsend. The nature of turbulent motion at large wave-numbers. *Proceedings of the Royal Society of London. Series A. Mathematical and Physical Sciences*, 199(1057):238–255, 1949.
- ¹⁰Roberto Benzi, Luca Biferale, R Fisher, DQ Lamb, and Federico Toschi. Inertial range eulerian and lagrangian statistics from numerical simulations of isotropic turbulence. *Journal of Fluid Mechanics*, 653:221–244, 2010.
- ¹¹Jérémie Bec, Samridhhi Sankar Ray, Ewe Wei Saw, and Holger Homann. Abrupt growth of large aggregates by correlated coalescences in turbulent flow. *Physical Review E*, 93(3):031102, 2016.
- ¹²Jérémie Bec, Holger Homann, and Samridhhi Sankar Ray. Gravity-driven enhancement of heavy particle clustering in turbulent flow. *Physical review letters*, 112(18):184501, 2014.
- ¹³BJ Devenish, Peter Bartello, J-L Brenguier, LR Collins, Wojciech W Grabowski, RHA IJzermans, Szymon P Malinowski, MW Reeks, JC Vassilicos, L-P Wang, et al. Droplet growth in warm turbulent clouds. *Quarterly Journal of the Royal Meteorological Society*, 138(667):1401–1429, 2012.
- ¹⁴Gregory Falkovich, A Fouxon, and MG Stepanov. Acceleration of rain initiation by cloud turbulence. *Nature*, 419(6903):151–154, 2002.
- ¹⁵James J Riley, Ralph W Metcalfe, and Michael A Weissman. Direct numerical simulations of homogeneous turbulence in density-stratified fluids. In *AIP Conference Proceedings*, volume 76, pages 79–112. American Institute of Physics, 1981.
- ¹⁶Fabio Feraco, Raffaele Marino, Alain Pumir, Leonardo Primavera, Pablo Daniel Mininni, Annick Pouquet, and Duane Rosenberg. Vertical drafts and mixing in stratified turbulence: Sharp transition with froude number. *Europhysics Letters*, 123(4):44002, 2018.
- ¹⁷C Rorai, Pablo Daniel Mininni, and A Pouquet. Turbulence comes in bursts in stably stratified flows. *Physical Review E*, 89(4):043002, 2014.
- ¹⁸Cecilia Rorai, Pablo Daniel Mininni, and A Pouquet. Stably stratified turbulence in the presence of large-scale forcing. *Physical Review E*, 92(1):013003, 2015.
- ¹⁹Jackson R Herring and Olivier Métais. Numerical experiments in forced stably stratified turbulence. *Journal of Fluid Mechanics*, 202:97–115, 1989.
- ²⁰Yoshifumi Kimura and JR Herring. Energy spectra of stably stratified turbulence. *Journal of fluid mechanics*, 698:19–50, 2012.
- ²¹P Caulfield Colm-cille. Open questions in turbulent stratified mixing: do we even know what we do not know? *Physical Review Fluids*, 5(11):110518, 2020.
- ²²Arun Kumar Varanasi and Ganesh Subramanian. Motion of a sphere in a viscous density stratified fluid. *Journal of Fluid Mechanics*, 949:A29, 2022.
- ²³M Van Aartrijk, HJH Clercx, and KB Winters. Single-particle, particle-pair, and multiparticle dispersion of fluid particles in forced stably stratified turbulence. *Physics of Fluids*, 20(2), 2008.
- ²⁴Luca Biferale, Guido Boffetta, Antonio Celani, Alessandra Lanotte, and Federico Toschi. Lagrangian statistics in fully developed turbulence. *Journal of Turbulence*, (7):N6, 2006.
- ²⁵Sagar Chakraborty, Uriel Frisch, and Samridhhi Sankar Ray. Extended self-similarity works for the burgers equation and why. *Journal of Fluid Mechanics*, 649:275–285, 2010.
- ²⁶Roberto Benzi and Federico Toschi. Lectures on turbulence. *Physics Reports*, 1021:1–106, 2023.
- ²⁷Arun Kumar Varanasi, Navaneeth K Marath, and Ganesh Subramanian. The rotation of a sedimenting spheroidal particle in a linearly stratified fluid. *Journal of Fluid Mechanics*, 933:A17, 2022.
- ²⁸Prateek Anand, Samridhhi Sankar Ray, and Ganesh Subramanian. Orientation dynamics of sedimenting anisotropic particles in turbulence. *Physical Review Letters*, 125(3):034501, 2020.
- ²⁹Jérémie Bec, Stefano Musacchio, and Samridhhi Sankar Ray. Sticky elastic collisions. *Physical Review E—Statistical, Nonlinear, and Soft Matter Physics*, 87(6):063013, 2013.